science.sciencemag.org/content/364/6438/386/suppl/DC1

Supplementary Materials for

Nitrogen isotope evidence for expanded ocean suboxia in the early Cenozoic

Emma R. Kast*, Daniel A. Stolper, Alexandra Auderset, John A. Higgins, Haojia Ren, Xingchen T. Wang, Alfredo Martínez-García, Gerald H. Haug, Daniel M. Sigman

*Corresponding author. Email: ekast@princeton.edu

Published 26 April 2019, *Science* **364**, 386 (2019)
DOI: 10.1126/science.aau5784

This PDF file includes:

Other Supplementary Material for this manuscript includes the following:
(available at science.sciencemag.org/content/364/6438/386/suppl/DC1)

Data S1 and S2 (.xlsx)

Materials and Methods

Sites and Age Models

Samples are from the Ocean Drilling Program (ODP) or International Ocean Discovery Program (IODP). Cores were sampled approximately every other section (each section is a 1.5m interval). The age model for Site 1209 is based on planktonic foraminifera (*50*) and calcareous nannofossil (*51*) biostratigraphy, for Site 1263 on planktonic foraminifera and calcareous nannofossil biostratigraphy (*20*) as well as paleomagnetic reversals (*52*), and for Site U1409 on planktonic foraminifera, calcareous nannofossil, and radiolarian biostratigraphy as well as paleomagnetic reversals (*21*). Absolute age of datums for Site 1209 and Site 1263 were updated to those in the GTS2012 time scale (*47*) while age for datums at Site U1409 was already on the GTS2012 time scale. Ages were calculated by fitting a smoothed curve to the available datums for each site.

Site locations, paleolatitude estimates, and descriptions are given in Fig. 1 and Table S1. Their paleo-locations were tropical, subtropical, or temperate regions where nitrate is completely consumed at the surface in the modern ocean. None of the sites were polar or subpolar, equatorial, or within a coastal upwelling system during the time period covered by this study. Thus, these sites would have been characterized by complete nutrient consumption throughout the periods covered by our records; this largely avoids the potential for isotopic variation due to incomplete nitrate consumption. Water column denitrification and N_2 fixation are both focused in the low latitudes (*1, 7*), so the larger amplitude of $\delta^{15}N$ change at Site 1209 than at the other two core sites, with a higher Paleocene value and a lower middle Eocene value, may be due in part to its lower paleolatitude. For example, there is evidence for a low $\delta^{15}N$ of shallow thermocline nitrate in the subtropical North Pacific likely mostly due to N_2 fixation in surface waters (*53*), which may help to explain the observation of lower FB-$\delta^{15}N$ at Site 1209 than Sites 1263 and U1409 during the middle Eocene (Fig. 1). Spatial patterns in the shallow subsurface nitrate $\delta^{15}N$ and in surface sediment FB-$\delta^{15}N$ have not yet been clearly defined for the modern North Pacific subtropical gyre. As a result, we cannot rule out an influence on Site 1209 FB-$\delta^{15}N$ from the northwestward movement of this site over the early Cenozoic. However, the amplitude of FB-$\delta^{15}N$ change in the Site 1209 record is greater than the modern spatial range of approximately 5‰ in FB-$\delta^{15}N$ in the region observed in work to date (*54*, *55*). Furthermore, the similar timing of the downcore changes with the Atlantic records provides additional evidence that the major FB-$\delta^{15}N$ changes at Site 1209 are not dominated by migration of the site across different oceanographic regimes.

Foraminifera-bound and bulk sediment organic matter $\delta^{15}N$ measurement

Bulk sediment was wet-sieved into >250 μm, 125-250 μm, and <125 μm size fractions and dried at 60°C. A subset of the >250 μm and 125-250 μm size fractions were examined and are composed almost entirely of planktonic foraminifera. Approximately 20 mg of each >250 μm and 125-20 μm size fraction (which we refer to as "mixed foraminifera") were weighed out, gently crushed between a glass petri dish and watch glass, and transferred to 15 ml centrifuge tubes. For genus-specific measurements, approximately 10 mg of individuals representing the genera *Acarinina* and *Morozovella* were picked from the >250 μm size fraction of targeted intervals.

Crushed mixed foraminifera and picked foraminifera were cleaned before analysis following protocols given in (*14*, *17*). Briefly, crushed powders were sonicated for 2-3 minutes with 10 ml of a 2% sodium polyphosphate solution adjusted to pH 8, to remove clays and similar

contaminants. The sodium polyphosphate solution was then decanted, samples were rinsed three times with deionized water (DIW), and 10 ml of a solution of dithionite and citric acid, adjusted to pH 8, was added. Samples were placed in an 80°C water bath for 1 hour, with intermittent shaking. This step reduces oxidized contaminants, such as metal oxide coatings, to more soluble forms that can then be washed away (*56*). The solution was decanted, and samples were rinsed three times with DIW and transferred to combusted 12 ml glass vials. Next, 5 ml of a basic potassium persulfate solution (recipe: 2 g sodium hydroxide + 2 g potassium persulfate per 100 ml DIW water) was added to the samples, and they were autoclaved for 65 minutes at 120°C. This step oxidizes any external organic matter and dissolves most of any siliceous material that may be present in the mixed foraminifera samples. The oxidizing solution was removed, samples were rinsed 5 times with DIW, and excess water was removed. Samples were then dried overnight at 60°C. With every batch of samples being cleaned, an in-house coral carbonate standard was included to track long-term reproducibility.

After cleaning, samples were dissolved and oxidized to nitrate (*17*, *57*) and then analyzed for nitrogen isotopic composition with the denitrifier method (*58*, *59*) as follows. For mixed foraminifera and picked foraminifera samples, 5-10 mg of cleaned powders were weighed into 4 ml combusted glass vials. For bulk sediment measurements, 15-20 mg of bulk sediment was weighed into 4 ml pre-combusted vials, without any pretreatment. Powders were dissolved by addition of 80 µl of 4N hydrochloric acid. Organic N was oxidized to nitrate by reaction with 1 ml of basic potassium persulfate solution. The persulfate solution recipe is 1 g of 4-times recrystallized low N potassium persulfate and 2 g sodium hydroxide in 100 ml of low-temperature distilled DIW and was made immediately before use. Samples were autoclaved for 1 hour at 120°C to ensure complete oxidation, as the oxidizing power of the persulfate reagent is heightened at high temperature (*60*). To address the effect of these procedures on the final measured $\delta^{15}N$ values, a series of amino acid isotope references and blanks were oxidized concurrently with the samples. USGS40 and USGS65 have assigned $\delta^{15}N$ values of -4.5‰ and 20.68‰, respectively (*61*, *62*) . Aliquots of these references with N content ranging from 5 to 50 nmol were treated identically to the samples, and the deviations from true $\delta^{15}N$ values for varying N content are used to calculate the $\delta^{15}N$ of the blank. These amino acid references also serve as a check to ensure that oxidation of the samples went to completion.

The high pH of the persulfate oxidation step also precipitates the dissolved calcium. After oxidation, the sample was centrifuged at 6000 rpm for 10 minutes and the supernatant containing the sample nitrate was transferred to a new pre-combusted 4 ml vial. The pH of the samples was adjusted to 5-7 by additions of 4N hydrochloric acid. Nitrate concentration in the sample was measured by Vanadium(III) reduction and chemiluminescence with a Teledyne NO_x analyzer to determine the appropriate volume of sample to aliquot for isotopic analysis (*63*).

Isotopic composition and N content were measured using the 'denitrifier method', in which nitrate is quantitatively converted to N_2O by denitrifying bacteria that lack N_2O reductase activity (*58*). The N_2O is subsequently purified, concentrated, and analyzed for $\delta^{15}N$ by a purpose-built preparation system in line with a MAT 253 gas-source stable isotope ratio mass spectrometer (*59*). Isotope values are reported relative to air through calibration with two nitrate isotopic references, IAEA-N3 and USGS-34 with known $\delta^{15}N$ values of 4.7‰ and -1.8‰, respectively (*64*). The in-house coral standard run with all sample batches provides a measure of long-term reproducibility, which was 0.25‰ (1σ) over the course of this study. Replicates, beginning at the oxidation step, were measured for approximately a third of the > 250 µm size fraction samples, and representative errors for these replications are given in Fig. 1.

TEX_{86} measurement

Samples were freeze-dried and extracted using a Thermo ASE350 with a mixture of dichloromethane and methanol (DCM:MeOH 9:1). The extracts were dried in a centrifugal evaporator ("Rocket" by Genevac) and purified over 5% deactivated silica column (Sigma Aldrich, pore size 60 Å, particle size of 63-200 µm, 70-230 mesh) by collecting the eluting compounds with hexane, and subsequently with DCM:MeOH (1:1). 60 µl of internal standard (C_{46}-GDGT, synthesized by (*65*)) was added to the glycerol dialkyl glycerol tetraether (GDGT) fraction for quantification purposes (*66*). The polar fraction, containing the GDGTs, was filtered through a PTFE filter (0.4 µm pore size) with a 98.2:1.8 mixture of hexane:isopropanol (hex:IPA).

Chromatographic separation and quantification of GDGTs was performed with an HPLC (Agilent 1260 Infinity) coupled to a single quadrupole mass spectrometer (Agilent 6130) following the methods given in (*67*). Briefly, separation of the compounds was achieved using two ultra-high performance liquid chromatography (UHPLC) silica columns connected in series (BEH HILIC columns, 2.1x150 mm, 1.7 µm; Waters) coupled to a pre-column (2.1x150 mm, Waters) and maintained at 30°C. The compounds were eluted isocratically with a 1.8% IPA in hexane mixture for the first 25 min, followed by a gradient to 3.5 % IPA in hexane in 25 min, and a column cleaning step with 10 % IPA in hexane. The flow was kept constant at 0.2 ml/min during the entire run.

Sea surface temperatures (SSTs) were calculated using the TEX^{H}_{86} calibration from (*68*) (equations 1 and 2), which is recommended for reconstructing SSTs > 15ºC, such as those temperatures characteristic for the Eocene and Paleocene. GDGT-1, GDGT-2 and GDGT-4 refer to GDGTs containing 1, 2 and 3 cyclopentane moieties. Cren' indicates the regio-isomer Crenarchaeol.

$$TEX^{H}_{86} = \log(([GDGT\text{-}2]+[GDGT\text{-}3]+[Cren'])/([GDGT\text{-}1]+[GDGT\text{-}2]+[GDGT\text{-}3]+[Cren'])) \quad (1)$$

$$SST(ºC)=68.4(TEX^{H}_{86})+38.6 \quad (2)$$

In order to test for potential influences of the calibration on the reconstructed temperatures, we also use the BAYSPAR calibration proposed by (*48*). BAYSPAR consists of a Bayesian model developed to predict SSTs from TEX_{86} values, considering the spatially varying trends in the response of TEX_{86} to temperature. For the different TEX_{86} SST calibrations, the temperature trend and absolute values are within calibration uncertainties (fig. S7d).

Evaluation of non-thermal influences on TEX_{86}

In order to assess the robustness of the observed SST changes at ODP Site 1209, we evaluated potential influences of secondary, non-thermal effects on GDGT distribution, such as degradation, thermal alteration, terrestrial input and methanogenesis (fig. S7). Table S3 summarizes the indices used, the recommended thresholds, and references. These values are also provided in Data Table S2.

The BIT index uses the ratio of the most abundant branched GDGTs (brGDGTs) to Crenarchaeol (Cren) and describes the relative input of soil organic matter delivered to the marine environment (*69*). (*70*) suggests that SST values be excluded where TEX_{86} estimates are

associated with BIT indices >0.3 (fig. S7a). None of the samples analyzed are above this threshold, with a maximum BIT of 0.13.

The primary TEX_{86}-SST signal can be modified by the introduction of compounds synthesized by sedimentary methanogenic and methanotrophic archaea (*71*). We estimate the contribution of sedimentary archaeal methanogen-synthesized GDGTs to the sedimentary GDGT pool using %GDGT-0 (*72*). None of our values is above the 67% threshold (maximum value is 55%) used to identify significant contribution by methanogenic and methanotrophic archaea to the TEX_{86} signal (fig. S7b).

The methane index (MI) is used to characterize anaerobic oxidation of methane in either gas hydrates or methane-rich deep-sea environments. This index compares the relative input of methanotrophic Euryarchaeota (which produce predominantly GDGT-0, -1, -2) versus ammonia-oxidizing Thaumarchaeota, producing Cren and Cren′ (*73*). Hydrate-impacted sediments are reflected by high MI values (MI > 0.5) and should be removed accordingly (*74*) (fig. S7c). Our data shows no evidence of methanotrophic activity as MI values are all below 0.35.

The Ring Index can help identify samples that may have been influenced by non-thermal factors and/or deviate from the SST-TEX_{86} relationship found in modern analogues. By looking at the weighted average of the ring numbers in GDGT compounds, one can distinguish samples with GDGT distributions that differ from those found in the modern core-top dataset used to calibrate TEX_{86} to SST (*75*). By applying the recommended exclusion criteria, we detect only 4 data points of the TEX_{86} dataset (a total of 46 data points) from ODP Site 1209 that lie outside the recommended value (fig. S7e).

The low BIT, %GDGT-0 and MI indicate that the sediment was not affected by terrestrial input of GDGTs or methanogenic activity in the sediment. The ΔRI identifies 4 samples with offsets greater than the recommended value, potentially indicating that non-thermal factors could have contributed to the GDGT distribution in those samples. However, this seems unlikely given the low values obtained for all the other GDDT indices and the similarity of the reconstructed SST for adjacent samples with ΔRI values within the recommended range (red and grey symbols in fig. S7d). Accordingly, those 4 samples were not excluded.

N flux calculations

We calculated water column and sedimentary denitrification fluxes for each main period of stable $\delta^{15}N$ (Oligocene, <33 Ma ago; middle Eocene, 43 – 50 Ma ago; and Paleocene, 56 – 62 Ma ago) using a one-box, steady state isotope mass balance of mean ocean nitrate $\delta^{15}N$, with N_2 fixation as the input ($\delta^{15}N$ = -1‰)(*8*, *9*) and two outputs: denitrification in the water column (with an isotope effect of 20‰) (*11*) and sediments (with no fractionation)(*10*). We employed five main assumptions. (i) N fluxes in the Oligocene are similar to modern. Our basis for this is that FB-$\delta^{15}N$ over this time frame is similar to core-top FB-$\delta^{15}N$ at the core sites (Fig. 1). (ii) Water column denitrification was not focused in the Atlantic, such that the average of the two Atlantic FB-$\delta^{15}N$ records provide a reasonable starting point for approximating mean ocean nitrate $\delta^{15}N$. (iii) We apply a shallow subsurface to deep ocean nitrate $\delta^{15}N$ offset of 2‰, such that the calculated mean ocean nitrate $\delta^{15}N$ at each interval is 2‰ lower than the average FB-$\delta^{15}N$ value. This is based on modern observations of ocean nitrate $\delta^{15}N$ (*7*) and the 2‰ elevation of core-top FB-$\delta^{15}N$ at these sites over modern mean ocean nitrate $\delta^{15}N$ (7‰ *vs.* 5‰). (iv) The $\delta^{15}N$ change from middle Eocene to Oligocene is entirely driven by a change in sedimentary denitrification flux. (v) The $\delta^{15}N$ change from Paleocene to middle Eocene is entirely driven by a change in the water column denitrification flux. Based on the mean ocean nitrate $\delta^{15}N$ estimated

from assumption (iii) and the average FB-δ^{15}N of each time slice, the ratio of water column to total denitrification, F_{wc}, is calculated. F_{wc} = 1 indicates that 100% of denitrification occurred in the water column. Based on assumption (i), water column denitrification in the Oligocene is set to modern estimates of 60 Tg N/yr (*43*). From the water column denitrification flux and F_{wc}, sedimentary and total denitrification are calculated for the Oligocene. Eocene water column, sedimentary, and total denitrification are then calculated from F_{wc}, assumption (iv), and previously calculated Oligocene fluxes. Similarly, Paleocene N fluxes are calculated from F_{wc}, assumption (v), and the calculated Eocene fluxes. Errors are propagated throughout the calculations, starting with the standard deviation (σ) of the FB-δ^{15}N for each time interval.

To address the sensitivity of this calculation to the records that we use to approximate mean ocean nitrate and to the isotope effect assumed for water column denitrification, we perform the same calculation under a variety of scenarios (Table S4). We vary the isotope effect of water column denitrification (ε_{wcd}) from 10 to 25‰, as recent studies have suggested a lower ε_{wcd}, down to 10‰, under ocean relevant conditions (*76*–*78*). Using an ε_{wcd} value of 10‰ versus 20‰ yields a greater change in water column and total denitrification from the Oligocene to the Paleocene, while the change in sedimentary denitrification remains similar across the ε_{wcd} range of 15‰ to 25‰.

Supplementary Text

Role of diagenesis in FB-δ^{15}N records

From studies of the Pleistocene glacial cycles, multiple lines of evidence point to the robust protection of foraminifera-bound organic N against diagenesis (*54*, and references therein). However, given that this is the first application of FB-δ^{15}N extending back tens of millions of years, the potential role of diagenesis on the record warrants consideration. An effect from diagenesis cannot be uniformly precluded for any paleoceanographic proxy. Moreover, a correlation between FB-δ^{15}N and FB-N content is observed in each of the three records reported here (Figs. S8 and S9). Nevertheless, the existing data do not point to diagenetic change as the driver of the major δ^{15}N changes in the records. Below, this point is pursued through: (A) comparison of fossil FB-N content with modern and core-top ranges, (B) consideration of previous work on the effects of diagenesis on FB-δ^{15}N in the context of the early Cenozoic records, (C) comparison of the changes in FB-δ^{15}N and FB-N content and their consistency among sites with previous findings on the effect of diagenesis on N isotopes, and (D) comparison of the down-core FB-δ^{15}N changes with other sedimentary properties.

(A) In the current study, the N content of the mixed foraminifera ranges from 1 to 4 µmol/g, similar to the range of 1-5 µmol/g observed in surface sediment foraminifera (*15*). This suggests that, despite the apparent recrystallization of foraminiferal carbonate in deep sea sediments on million-year time scales (*79*), a large fraction of the original shell-bound N survives. We consider this a somewhat surprising result, given the effects of recrystallization on most foraminiferal calcite-based proxies in Cenozoic sediments (e.g., δ^{18}O) (*80*), that bodes well for a range of potential applications of foraminifera-bound organic matter.

(B) A ground-truthing study near Bermuda suggests that foraminifera-bound N loss during early seafloor diagenesis does not occur with significant isotope fractionation (*15*). Given the chemically labile, amino acid-dominated composition of FB-N (*23*, *24*), this observation is consistent with the expectation that any newly exposed N will be completely lost rather than isotopically altered and re-incorporated in recrystallized foraminifera (*15*). This suggests that the

correlation between FB-$\delta^{15}N$ and FB-N content observed in the current study is not the result of diagenetic alteration.

(C) We compared the FB-$\delta^{15}N$ and FB-N content and observed a positive correlation (fig. S9). In studies of diagenesis, almost all observations point to the potential for $\delta^{15}N$ elevation of the remaining N due to preferential degradation of ^{14}N-containing N, which would result in a negative correlation between $\delta^{15}N$ and N content (*16*). The correlation observed in the present study is of higher FB-$\delta^{15}N$ in association with higher FB-N content, the opposite of this expectation. The observed relationship thus argues against a role for diagenesis.

The structure of the FB-$\delta^{15}N$ records themselves makes a further argument against the role of diagenesis. No single direction of change with age is observed: proceeding down-core, FB-$\delta^{15}N$ and FB-N content is higher in the Oligocene, lower in the Eocene, then higher again in the Paleocene (Fig. 1 and fig. S8). To achieve this result, whatever alteration process is occurring would need to be changing over time, in an identical way at all three sites. In order to explain our records, this would necessitate two synchronous, global ocean-scale changes in the diagenetic process of mineral bound organic matter.

(D) Comparison of the FB-$\delta^{15}N$ records with the sediment composition of each core shows no consistent correlations, either with depth within a core or between cores. As an example, the records of FB-$\delta^{15}N$ show no correspondence with $CaCO_3$ wt. % at each site (fig. S10). If diagenetic changes were responsible for the FB-$\delta^{15}N$ changes, a connection to sedimentary properties would be expected, but none is observed.

The combination of these lines of evidence indicates that diagenesis is not driving the FB-$\delta^{15}N$ changes reported in this study. The processes underlying the downcore changes in FB-N content remain an open question. Roles for primary conditions in both the surface and deep ocean are being explored with modern observations and core-top materials.

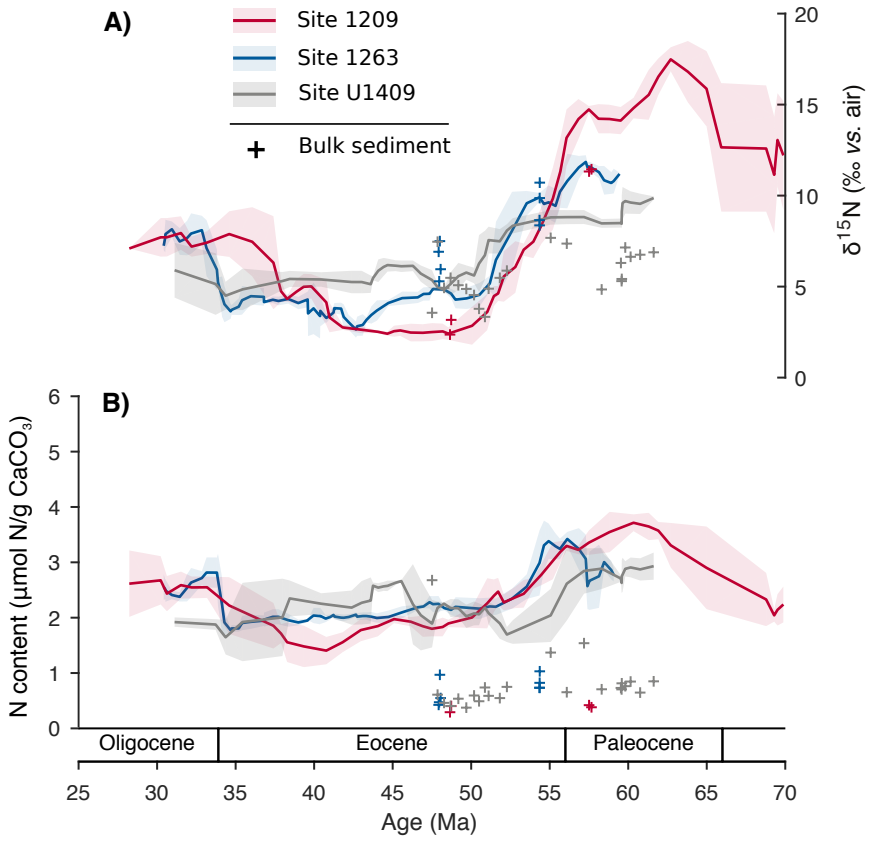

Fig. S1.

The (A) $\delta^{15}N$ and (B) N content of bulk sediment (crosses) for Site 1209 (red), Site 1263 (blue), and Site U1409 (grey). Lines and shaded intervals represent the moving average of our mixed FB-$\delta^{15}N$ and FB-N content records, as in Fig. 1 and fig. S8. Based on this subset of samples, bulk sediment $\delta^{15}N$ appears to capture to first order the same changes as FB-$\delta^{15}N$ at Site 1209 and Site 1263, although the Paleocene to Eocene $\delta^{15}N$ decline appears muted in the bulk sediment. At Site U1409 where the FB-$\delta^{15}N$ change is less dramatic, it is less clear whether bulk sediment $\delta^{15}N$ tracks FB-$\delta^{15}N$. At all sites, the N content of the bulk sediment is much lower than the mixed foraminifera. The low N content of the bulk sediment in the same samples suggests that if shell-bound N had been exposed, it would have been lost. The low N content of bulk sediment also raises the possibility that the foraminifera-bound N is the main reservoir of organic N in these sediments, particularly at Site 1209 and Site 1263. The samples analyzed here suggest that $\delta^{15}N$ measurement of bulk sedimentary N can potentially recover information about the past ocean N cycle. However, at this low N content, bulk sedimentary $\delta^{15}N$ is highly susceptible to modification by exogenous sedimentary materials with higher N content. Moreover, bulk sediment could be easily contaminated during coring and sampling, which may explain the lower $\delta^{15}N$ change through the Paleocene to Eocene that we measure in the bulk sediment and the lack of correspondence between bulk sediment $\delta^{15}N$ and FB-$\delta^{15}N$ at Site U1409. Standard Dumas combustion-based methods are not adequately sensitive to measure the $\delta^{15}N$ of this material (by roughly an order of magnitude), such that the high sensitivity methods used for foraminifera-bound N were also used for the bulk sediment measurements reported here.

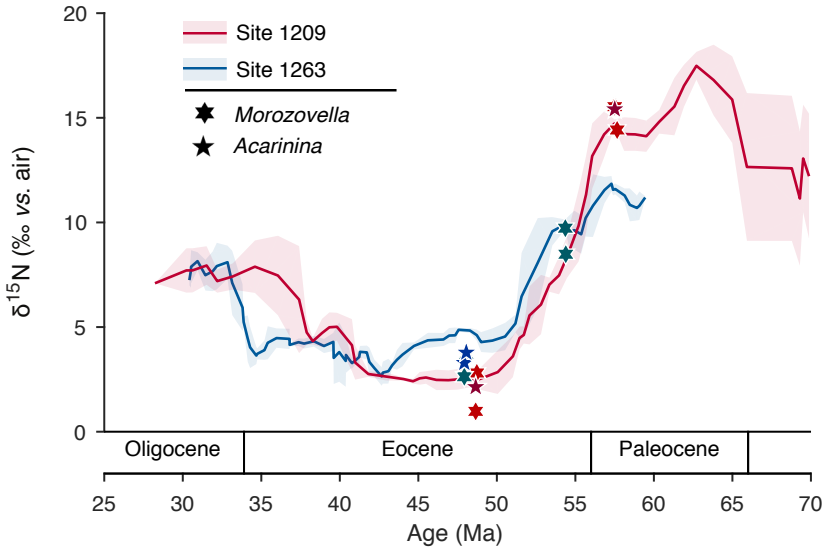

Fig. S2

Genus specific FB-δ^{15}N compared with the data from mixed foraminifera, for Site 1209 (red) and Site 1263 (blue). Genus *Morozovella* is shown in six-pointed stars, genus *Acarinina* by five-pointed stars. Lines and shaded intervals represent the moving average of mixed FB-δ^{15}N record, as in Fig. 1. Foraminifera species with different physiologies and depth habitats are known to have different δ^{15}N. Most distinctly, symbiont-bearing euphotic zone foraminifera tend to have a δ^{15}N 1-2‰ lower than asymbiotic foraminifera (*14*). Previous measurements of modern foraminifera show typical species differences of ≤3‰ (*14*, *17*). This difference is small compared to the changes observed in our records. Moreover, the two genera that dominate our samples, *Morozovella* and *Acarinina*, have been diagnosed as symbiont-bearing (*81*). At both sites, genus-specific FB-δ^{15}N captures the large FB-δ^{15}N decrease during the early Eocene. Thus, the decline in mixed taxa FB-δ^{15}N cannot be attributed to genus-level changes in the community composition of foraminifera.

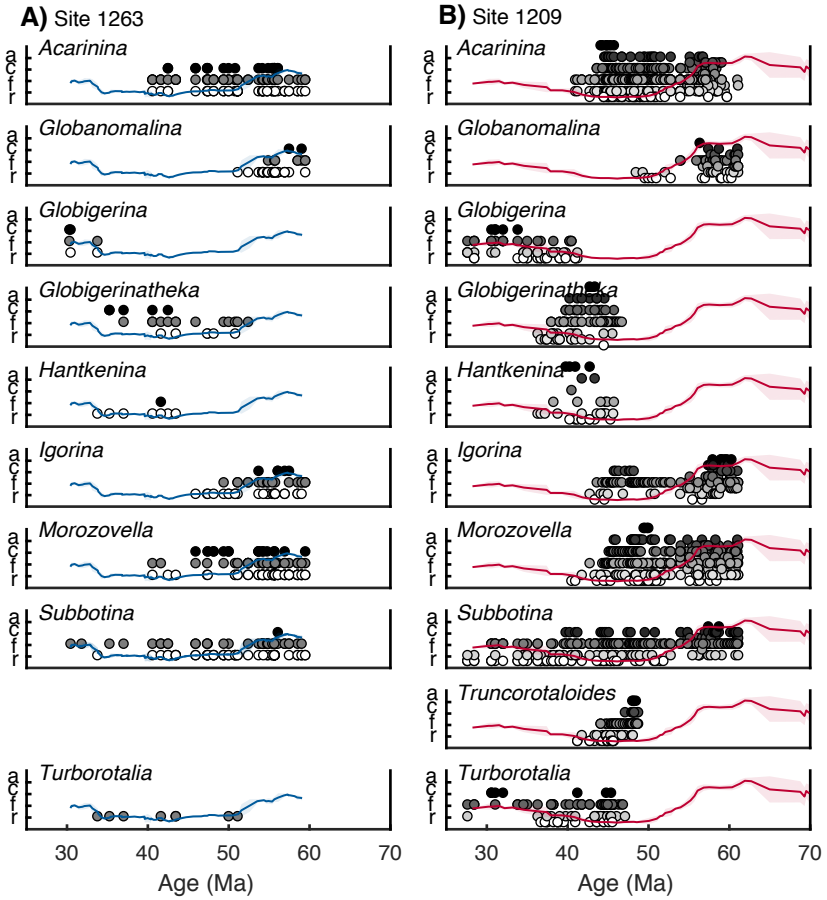

Fig. S3

Foraminifera abundance by genus over time for (A) Site 1263 and (B) Site 1209. Abundance of foraminifera as described in (*19*, *20*), from rare (r), few (f), common (c), abundant (a), with darker colors also representing greater abundance. FB-δ^{15}N record for each site as in Fig. 1 with a y-axis range from 0 to 20‰, to illustrate the timing of the major FB-δ^{15}N transition in the early Eocene between 57 and 50 Ma ago. These species abundance data do not show a major turnover in the represented genera between 57 and 50 Ma ago, which suggests the major FB-δ^{15}N change are not driven by genus-level changes in the community composition of foraminifera.

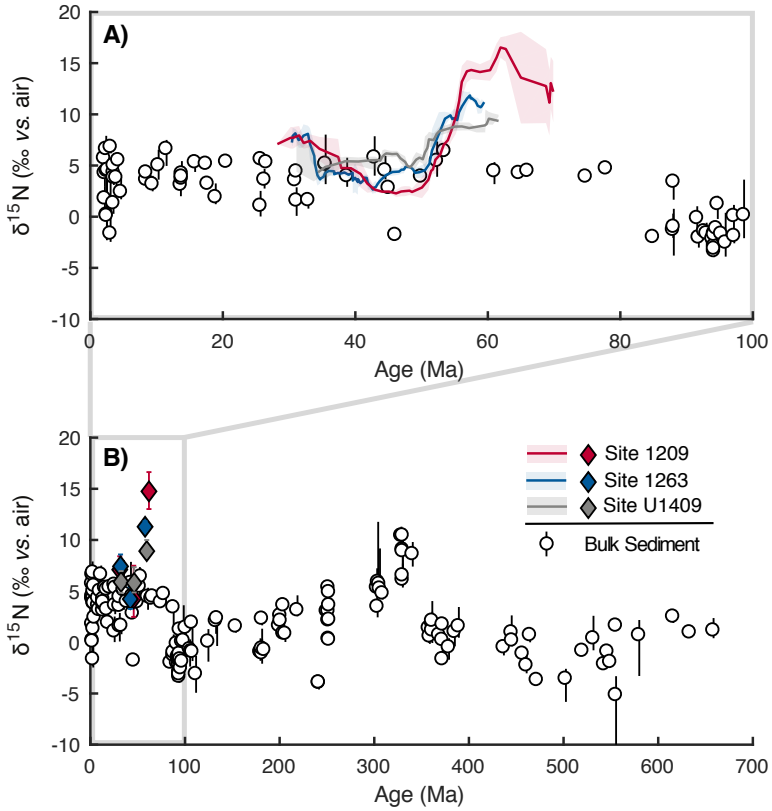

Fig. S4

Comparison of FB-$\delta^{15}N$ records with compilation of bulk sediment $\delta^{15}N$ from (*2*). Bulk sediment $\delta^{15}N$ records shown as in (*2*), plotted as mean $\delta^{15}N$ with the 16th-to-84th percentile range shown with the vertical bars. (A) FB-$\delta^{15}N$ records plotted as in Fig.1, (B) FB-$\delta^{15}N$ records plotted as mean $\delta^{15}N$ with the 16th-to-84th percentile range shown with the vertical bars for each time interval (Oligocene, Eocene, and Paleocene) for direct comparison with bulk sediment compilation. In the Paleocene, FB-$\delta^{15}N$ values and ranges fall outside previous observed bulk sediment $\delta^{15}N$ for the past 700 Ma. However, our high sensitivity bulk sedimentary N measurements (fig. S1) would display patterns similar to our FB-$\delta^{15}N$ measurements.

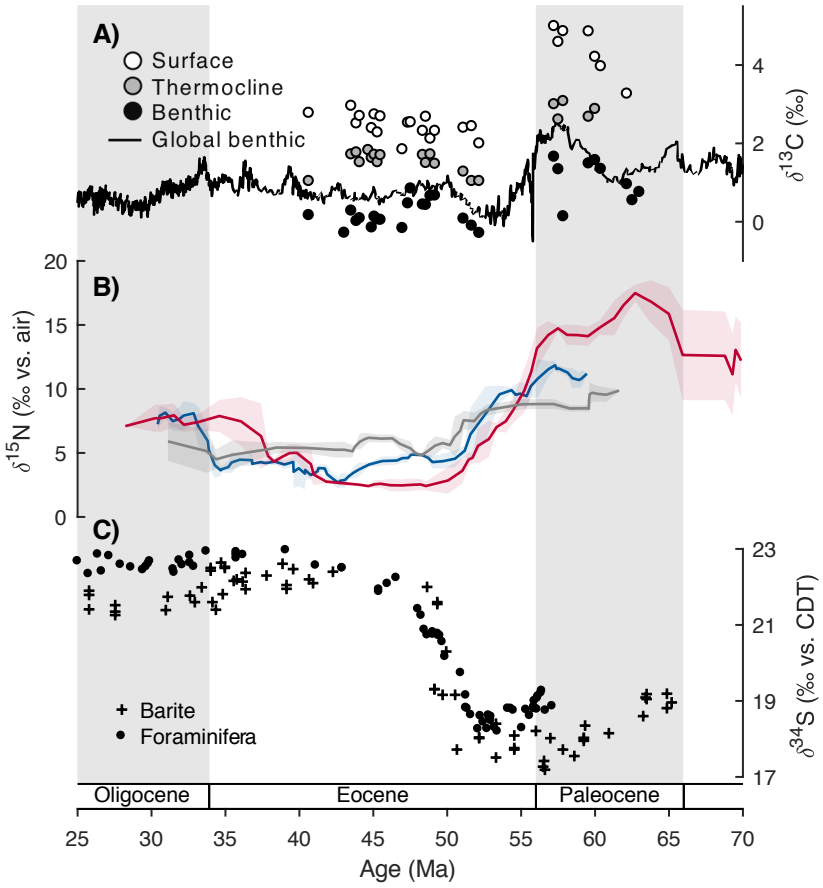

Fig. S5

Comparison of FB-$\delta^{15}N$ with foraminifera carbonate $\delta^{13}C$ and barite and foraminifera carbonate-associated sulfate $\delta^{34}S$ records across the early Cenozoic. (A) Ten-point moving mean of a global benthic foraminifera $\delta^{13}C$ compilation (*29*) and the $\delta^{13}C$ of putatively surface- and thermocline-dwelling planktonic foraminifera and benthic foraminifera from Site 1209 (*41*). (B) FB-$\delta^{15}N$ record as in Fig. 1. (C) The record of marine barite and foraminifera carbonate associated sulfate $\delta^{34}S$ (*37–39*). Grey regions show Paleocene and Oligocene intervals. The suggested bathymetric origin for the $\delta^{15}N$ change starting at 57 Ma is consistent with the marine barite $\delta^{34}S$ record, as the dramatic increase in the $\delta^{34}S$ record has been interpreted in terms of continental margin changes associated with the India-Asia collision (*39*) and occurs with similar timing to our $\delta^{15}N$ transition. The interpreted changes do not immediately provide an explanation for the peak in benthic foraminifera $\delta^{13}C$ at 57 Ma ago. However, the overall decrease in baseline benthic foraminifera $\delta^{13}C$ from the Paleocene to the Eocene may indicate a transition to lower organic matter burial, consistent with higher O_2 in the waters overlying the continental slopes, the latter representing major depocenters for organic carbon (*82*). As an important caveat, this interpretation does not take into account the expectation of a proposed negative feedback on the million year time scale, in which organic matter burial is stabilized through changes in atmospheric O_2 content (*83*). Nevertheless, the coincidence of the FB-$\delta^{15}N$ change with both the $\delta^{34}S$ and $\delta^{13}C$ records suggests that the combined bathymetric and circulation changes had wide-ranging ocean biogeochemical impacts.

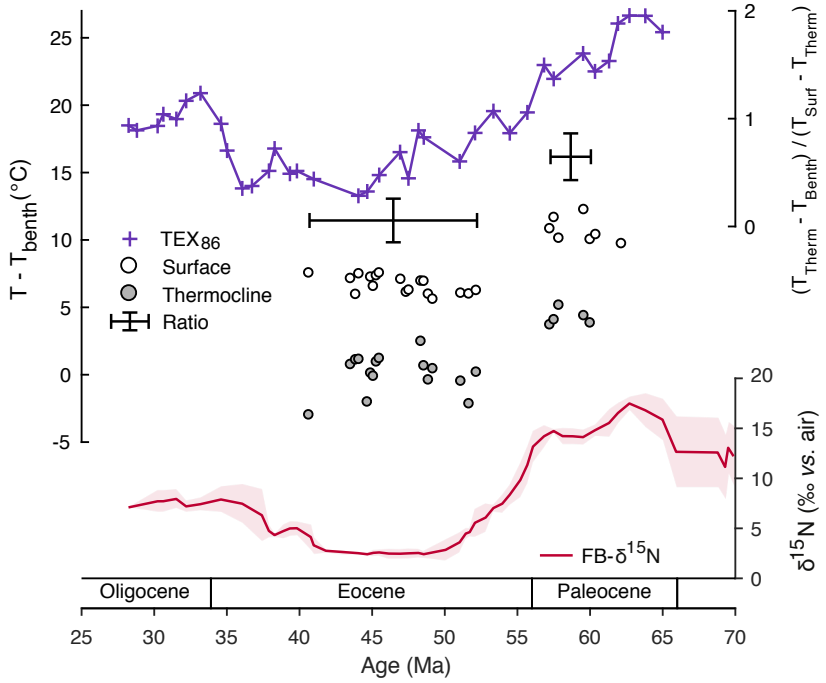

Fig. S6

Comparison of FB-δ^{15}N and reconstructed water column temperature gradient changes at Site 1209. Records of temperature for the surface ocean and thermocline, from TEX_{86} measurements (purple crosses) and foraminifera $\delta^{18}O$ (white circles)(*41*) at Site 1209, plotted as the difference from deep water temperatures reconstructed from a global compilation of benthic foraminifera $\delta^{18}O$ (*29*). The ratio of the thermocline-to-benthic temperature difference to surface-to-thermocline difference, from foraminifera $\delta^{18}O$ at Site 1209, is shown in black error bars plotted against the right axis, with higher values indicating a thermocline temperature more similar to the surface. Temperatures are as in Fig. 2 and the FB-δ^{15}N record as in Fig. 1. Surface dwelling foraminifera $\delta^{18}O$ temperature estimates are lower than TEX_{86} by ~10˚C, which may be due to diagenetic calcite recrystallization (*79*) and/or uncertainties in the TEX_{86} calibration. Regardless, differences in surface dwelling and benthic foraminifera $\delta^{18}O$ values lessen from 57 to 53 Ma ago at Site 1209, consistent with the decline in surface-to-deep temperature difference calculated using TEX_{86} as the sea surface temperature proxy. Moreover, between 57 and 53 Ma ago, the $\delta^{18}O$ of thermocline-dwelling planktonic foraminifera shifts from being more similar to surface dwellers to falling near to the benthic foraminifera. Both the reconstructed decline in surface-deep temperature difference and the apparent shift in the thermocline temperature toward deep water values after 57 Ma ago are consistent with low latitude-derived, warm salty waters ventilating the thermocline during the Paleocene, switching to high latitude ventilation during the Eocene.

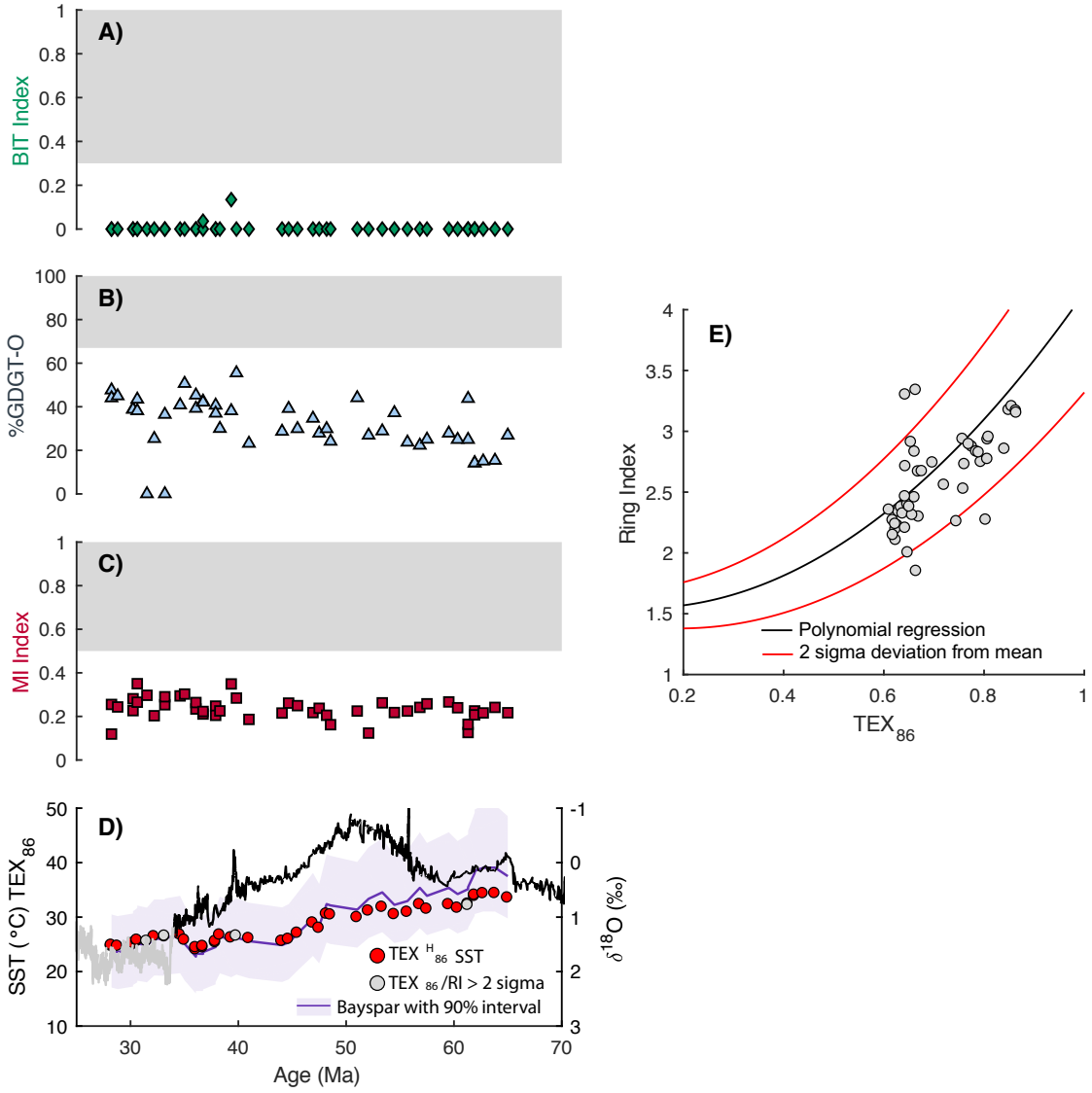

Fig. S7

Evaluation of non-thermal influences on TEX_{86} sea surface temperature reconstruction at ODP Site 1209. (A) Branched and isoprenoid tetraether index (BIT), (B) %GDGT-0, (C) methane index (MI), (D) SST reconstruction of ODP 1209. Red data points indicate TEX^{H}_{86} SST values where all the indices are within the recommended values, and in gray those with RI values outside the recommended range. Ten point moving average of benthic foraminifera $\delta^{18}O$ record from (*29*). The purple continuous line represents the SST reconstructed using the BAYSPAR calibration based on TEX_{86} with its 90% confidence interval in light purple. (E) TEX_{86} – RI relationship for ODP Site 1209 samples (grey circles), plotted together with a polynomial regression of the modern calibration core-top dataset (black line). Red lines illustrate the 2σ deviation from the mean regression values.

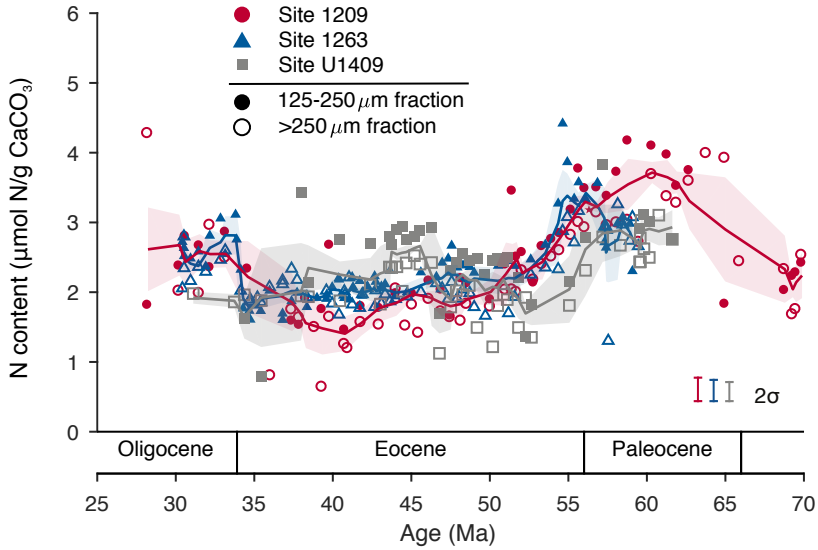

Fig. S8

FB-N content. Measurements are of the >250 µm (closed symbols) and 125-250 µm (open symbols) size fractions from Site 1209 (red circles), Site 1263 (blue triangles), and Site U1409 (grey squares). Correspondingly colored bold lines represent the 3-point moving average across both size fractions, with shaded uncertainty interval indicating its 1σ. Representative error bars show the average 2σ for replicates analyzed at each site.

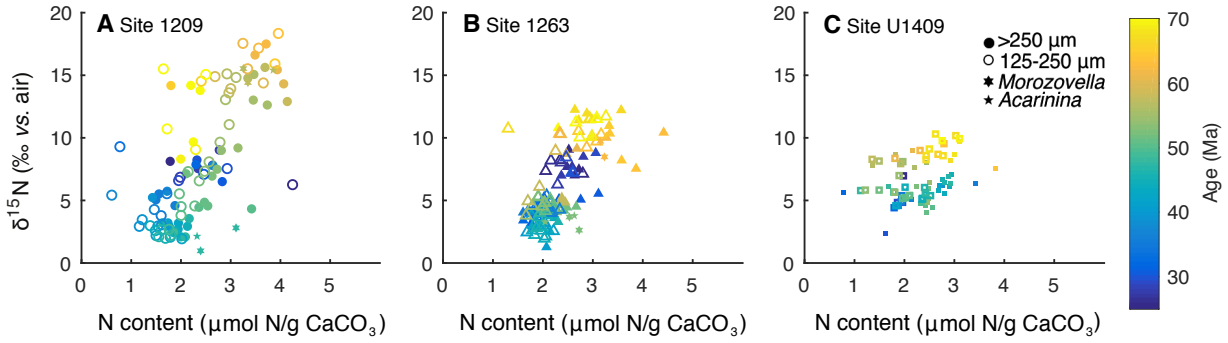

Fig. S9

FB-δ^{15}N *vs.* FB-N content for (A) Site 1209, (B) Site 1263 and (C) Site U109 for both >250 µm (closed symbols) and 125-250 µm (open symbols) size fractions. Symbols are colored by age. N content of the mixed foraminifera is correlated to FB-δ^{15}N, with higher FB-N content when FB-δ^{15}N is higher in the Paleocene/earliest Eocene and in the Oligocene.

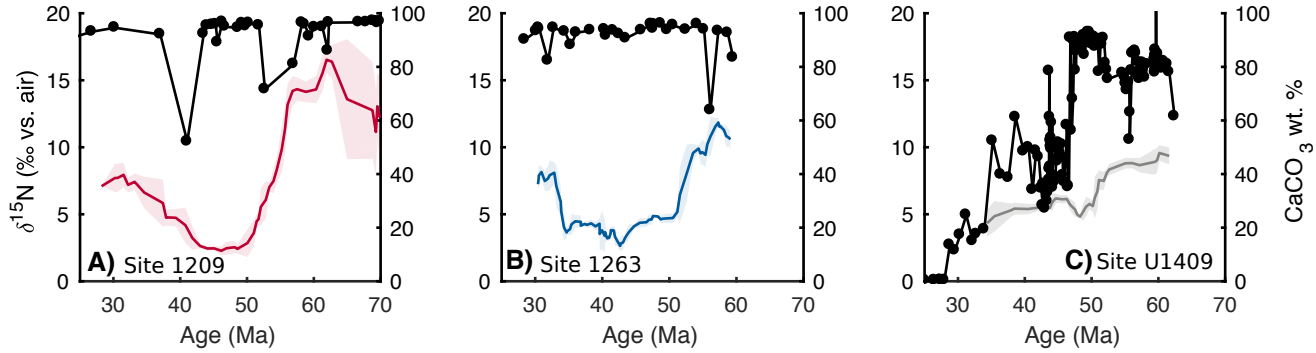

Fig. S10

Comparison of FB-$\delta^{15}N$ record with $CaCO_3$ wt. % for (A) Site 1209, (B) Site 1263, and (C) Site U1409. FB-$\delta^{15}N$ plotted on left axes, $CaCO_3$ wt. % plotted on the right axes and obtained from ODP and IODP Initial Reports (*19–21*).

Table S1.

Site locations. Data from (*19*) for Site 1209, (*20*) for Site 1263, (*21*) for Site U1409, except where otherwise indicated.

Site	Location Name	Depth (m)	Location (Modern)	Location (55 Ma ago)
1209	Shatsky Rise	2387	32.6517°N, 158.5060°E	12°N, 162.0°E
1263	Walvis Ridge	2717	28.5330°S, 2.7795°E	40°S (paleolatitude.org, *45*)
U1409	Newfoundland Ridge	3500	41.2958°N, 49.2333°W	31°N (paleolatitude.org, *45*)

Table S2.

N flux calculation results. Water column denitrification (WC), sedimentary denitrification (Sed), and total denitrification (Total) fluxes given in Tg N yr^{-1} where 1 Tg is 10^{12} g. Errors for calculations (σ) are the 1 standard deviation for each flux, as described in text.

Interval	**F_{WC}**	**σ_{FWC}**	**WC**	**σ_{WC}**	**Sed**	**σ_{Sed}**	**Total**	**σ_{Total}**
Oligocene	0.32	0.02	60	0	129	11	189	11
Middle Eocene	0.19	0.02	60	0	248	42	308	42
Paleocene	0.46	0.02	212	36	248	42	459	56

Table S3.

Summary of the indices used to evaluate non-thermal influences on the reconstructed TEX_{86} temperatures.

Name	Equation	Threshold	Ref.
Branched *vs.* Tetraether Index (BIT)	$\mathrm{BIT} = \frac{[I] + [II] + [III]}{[I] + [II] + [III] + [\mathrm{Cren}]}$	BIT < 0.3	(*69*)
%GDGT-0	$\%\mathrm{GDGT\text{-}0} = \left(\frac{[\mathrm{GDGT\text{-}0}]}{[\mathrm{GDGT\text{-}0}] + [\mathrm{Cren}]}\right) * 100$	%GDGT-0 < 67%	(*85*)
Methane Index (MI)	$\mathrm{MI} = \frac{[\mathrm{GDGT\text{-}1}] + [\mathrm{GDGT\text{-}2}] + [\mathrm{GDGT\text{-}3}]}{[\mathrm{GDGT\text{-}1}] + [\mathrm{GDGT\text{-}2}] + [\mathrm{GDGT\text{-}3}] + [\mathrm{Cren}] + [\mathrm{Cren'}]}$	MI < 0.5	(*74*)
Ring Index (ΔRI)	$\mathrm{RI} = 0 * \left(\frac{[\mathrm{GDGT\text{-}0}]}{\Sigma\mathrm{GDGT}}\right) + 1 * \left(\frac{[\mathrm{GDGT\text{-}1}]}{\Sigma\mathrm{GDGT}}\right) + 2 * \left(\frac{[\mathrm{GDGT\text{-}2}]}{\Sigma\mathrm{GDGT}}\right) + 3 * \left(\frac{[\mathrm{GDGT\text{-}3}]}{\Sigma\mathrm{GDGT}}\right) + 4 * \left(\frac{[\mathrm{Cren}]}{\Sigma\mathrm{GDGT}}\right) + 4 * \left(\frac{[\mathrm{Cren'}]}{\Sigma\mathrm{GDGT}}\right)$ $\mathrm{RI}_{\mathrm{TEX}} = -0.77(\pm 0.38) * \mathrm{TEX}_{86} + 3.32(\pm 0.34) * (\mathrm{TEX}_{86})^2 + 1.59(\pm 0.10)$ $\Delta\mathrm{RI} = \mathrm{RI}_{\mathrm{TEX}} - \mathrm{RI}_{\mathrm{sample}}$	-0.3 > ΔRI > 0.3	(*75*)

Table S4.

Comparison of N flux calculations using FB-$\delta^{15}N$ records from individual sites and averaging across sites, for a range of assumed values of water column denitrification isotope effects, ε_{wcd}. Water column denitrification (WC), sedimentary denitrification (Sed), and total denitrification (Tot) fluxes given in Tg N yr^{-1} where 1 Tg is 10^{12} g. Dash marks indicates where measured $\delta^{15}N$ and assumed ε_{wcd} do not yield a positive solution (i.e., with this calculation, a mean ocean nitrate $\delta^{15}N$ of > 10‰ cannot be achieved with an ε_{wcd} of 10‰). The bold fluxes represent the conditions used in the main text and Fig. 3 and are shown in detail in Table S2.

$\delta^{15}N$ record	Interval	ε_{wcd} = 10‰			ε_{wcd} = 15‰			ε_{wcd} = 20‰			ε_{wcd} = 25 ‰		
		WC	**Sed**	**Tot**	**WC**	**Sed**	**Tot**	**WC**	**Sed**	**Tot**	**WC**	**Sed**	**Tot**
Site 1209	**Oligocene**	60	33	93	60	80	140	60	126	186	60	173	233
	middle Eocene	60	347	407	60	550	610	60	754	814	60	957	1017
	Paleocene	--	347	--	5566	550	6116	1620	754	2374	1151	957	2108
Site 1263	**Oligocene**	60	29	89	60	73	133	60	117	177	60	162	222
	middle Eocene	60	128	188	60	221	281	60	315	375	60	409	469
	Paleocene	--	128	--	481	221	703	333	315	648	285	409	694
Site U1409	**Oligocene**	60	41	101	60	91	151	60	141	201	60	192	252
	middle Eocene	60	70	130	60	136	196	60	201	261	60	266	326
	Paleocene	311	70	381	161	136	297	138	201	339	129	266	395
Atlantic Average	**Oligocene**	60	34	94	60	81	141	**60**	**129**	**189**	60	176	236
	middle Eocene	60	94	154	60	171	231	**60**	**248**	**308**	60	325	385
	Paleocene	1100	94	1193	272	171	443	**212**	**248**	**459**	189	325	514
Overall Average	**Oligocene**	60	34	94	60	81	141	60	128	188	60	175	235
	middle Eocene	60	134	194	60	231	291	60	328	388	60	425	485
	Paleocene	--	134	--	574	231	805	377	328	705	318	425	743

Additional Data table S1 (separate file)

$\delta^{15}N$ and N content data. Sheet titled "MixedForamBound" contains all mixed foraminifera bound FB-$\delta^{15}N$ and FB-N content measurements. Columns highlighted in green are FB-$\delta^{15}N$ averages used for Fig. 1, columns highlighted in blue are FB-N content averages used in fig. S8. Sheet titled "PickedForamBound" contains all genera specific FB-$\delta^{15}N$ and FB-N content measurements, plotted in fig. S2. Sheet titled "BulkSedimentN" contains all bulk sediment $\delta^{15}N$ and N content measurements, plotted in fig. S1.

Additional Data table S2 (separate file)

TEX_{86} data for Site 1209. This table contains all TEX_{86} measurements, calculated indices, and temperature calculations. Column highlighted in green is the temperature calibration used in Fig. 2.

References and Notes

1. N. Gruber, “The marine nitrogen cycle: Overview and challenges” in *Nitrogen in the Marine Environment*, D. G. Capone, D. A. Bronk, M. R. Mulholland, E. J. Carpenter, Eds. (Elsevier, ed. 2, 2008), pp. 1–50.

2. T. J. Algeo, P. A. Meyers, R. S. Robinson, H. Rowe, G. Q. Jiang, Icehouse–greenhouse variations in marine denitrification. *Biogeosciences* **11**, 1273–1295 (2014). doi:10.5194/bg-11-1273-2014

3. Z. Liu, M. A. Altabet, T. D. Herbert, Plio-Pleistocene denitrification in the eastern tropical North Pacific: Intensification at 2.1 Ma. *Geochem. Geophys. Geosyst.* **9**, Q11006 (2008). doi:10.1029/2008GC002044

4. J. Zachos, M. Pagani, L. Sloan, E. Thomas, K. Billups, Trends, rhythms, and aberrations in global climate 65 Ma to present. *Science* **292**, 686–693 (2001). doi:10.1126/science.1059412 Medline

5. H. E. Garcia, L. I. Gordon, Oxygen solubility in seawater: Better fitting equations. *Limnol. Oceanogr.* **37**, 1307–1312 (1992). doi:10.4319/lo.1992.37.6.1307

6. See materials and methods in the supplement.

7. D. M. Sigman, F. Fripiat, “Ocean process tracers: Nitrogen isotopes in the ocean” in *Marine Biogeochemistry*, vol. 1 of *Encyclopedia of Ocean Sciences*, J. K. Cochran, H. Bokuniewicz, P. Yager, Eds. (Academic Press, ed. 3, 2019), pp. 263–278.

8. E. Wada, A. Hattori, Natural abundance of ^{15}N in particulate organic matter in the North Pacific Ocean. *Geochim. Cosmochim. Acta* **40**, 249–251 (1976). doi:10.1016/0016-7037(76)90183-6

9. A. N. Knapp, P. J. Difiore, C. Deutsch, D. M. Sigman, F. Lipschultz, Nitrate isotopic composition between Bermuda and Puerto Rico: Implications for N_2 fixation in the Atlantic Ocean. *Global Biogeochem. Cycles* **22**, GB3014 (2008). doi:10.1029/2007GB003107

10. J. A. Brandes, A. H. Devol, Isotopic fractionation of oxygen and nitrogen in coastal marine sediments. *Geochim. Cosmochim. Acta* **61**, 1793–1801 (1997). doi:10.1016/S0016-7037(97)00041-0

11. J. D. Cline, I. R. Kaplan, Isotopic fractionation of dissolved nitrate during denitrification in the eastern tropical north pacific ocean. *Mar. Chem.* **3**, 271–299 (1975). doi:10.1016/0304-4203(75)90009-2

12. C. Deutsch, D. M. Sigman, R. C. Thunell, A. N. Meckler, G. H. Haug, Isotopic constraints on glacial/interglacial changes in the oceanic nitrogen budget. *Global Biogeochem. Cycles* **18**, GB4012 (2004). doi:10.1029/2003GB002189

13. M. A. Altabet, “Isotopic tracers of the marine nitrogen cycle: Present and past” in *Marine Organic Matter: Biomarkers, Isotopes and DNA*, J. K. Volkman, Ed., vol. 2N of *The Handbook of Environmental Chemistry* (Springer, 2006), pp. 251–293.

14. H. Ren, D. M. Sigman, R. C. Thunell, M. G. Prokopenko, Nitrogen isotopic composition of planktonic foraminifera from the modern ocean and recent sediments. *Limnol. Oceanogr.* **57**, 1011–1024 (2012). doi:10.4319/lo.2012.57.4.1011

15. S. M. Smart, H. Ren, S. E. Fawcett, R. Schiebel, M. Conte, P. A. Rafter, K. K. Ellis, M. A. Weigand, S. Oleynik, G. H. Haug, D. M. Sigman, Ground-truthing the planktic foraminifer-bound nitrogen isotope paleo-proxy in the Sargasso Sea. *Geochim. Cosmochim. Acta* **235**, 463–482 (2018). doi:10.1016/j.gca.2018.05.023

16. R. S. Robinson, M. Kienast, A. Luiza Albuquerque, M. Altabet, S. Contreras, R. De Pol Holz, N. Dubois, R. Francois, E. Galbraith, T.-C. Hsu, T. Ivanochko, S. Jaccard, S.-J. Kao, T. Kiefer, S. Kienast, M. Lehmann, P. Martinez, M. McCarthy, J. Möbius, T. Pedersen, T. M. Quan, E. Ryabenko, A. Schmittner, R. Schneider, A. Schneider-Mor, M. Shigemitsu, D. Sinclair, C. Somes, A. Studer, R. Thunell, J.-Y. Yang, A review of nitrogen isotopic alteration in marine sediments. *Paleoceanography* **27**, PA4203 (2012). doi:10.1029/2012PA002321

17. H. Ren, D. M. Sigman, A. N. Meckler, B. Plessen, R. S. Robinson, Y. Rosenthal, G. H. Haug, Foraminiferal isotope evidence of reduced nitrogen fixation in the ice age Atlantic Ocean. *Science* **323**, 244–248 (2009). doi:10.1126/science.1165787 Medline

18. M. A. Altabet, W. B. Curry, Testing models of past ocean chemistry using foraminifera $^{15}N/^{14}N$. *Global Biogeochem. Cycles* **3**, 107–119 (1989). doi:10.1029/GB003i002p00107

19. Shipboard Scientific Party, "Site 1209" in *Proceedings of the Ocean Drilling Program, Initial Reports*, vol. 198 (ODP, 2002), chap. 5. doi:10.2973/odp.proc.ir.198.105.2002

20. Shipboard Scientific Party, "Site 1263" in *Proceedings of the Ocean Drilling Program, Initial Reports*, vol. 208 (ODP, 2004), chap. 4. doi:10.2973/odp.proc.ir.208.104.2004

21. R. D. Norris, P. A. Wilson, P. Blum, A. Fehr, C. Agnini, A. Bornemann, S. Boulila, P. R. Bown, C. Cournede, O. Friedrich, A. K. Ghosh, C. J. Hollis, P. M. Hull, K. Jo, C. K. Junium, M. Kaneko, D. Liebrand, P. C. Lippert, Z. Liu, H. Matsui, K. Moriya, H. Nishi, B. N. Opdyke, D. Penman, B. Romans, H. D. Scher, P. Sexton, H. Takagi, S. K. Turner, J. H. Whiteside, T. Yamaguchi, Y. Yamamoto, "Site U1409" in *Proceedings of the Integrated Ocean Drilling Program*, vol. 342 (IODP, 2014). doi:10.2204/iodp.proc.342.110.2014

22. See supplementary text in the supplement.

23. A. E. Ingalls, C. Lee, S. G. Wakeham, J. I. Hedges, The role of biominerals in the sinking flux and preservation of amino acids in the Southern Ocean along 170°W. *Deep-Sea Res. Part II* **50**, 713–738 (2003). doi:10.1016/S0967-0645(02)00592-1

24. K. King Jr., P. E. Hare, Amino acid composition of planktonic foraminifera: A paleobiochemical approach to evolution. *Science* **175**, 1461–1463 (1972). doi:10.1126/science.175.4029.1461 Medline

25. J. A. Brandes, A. H. Devol, A global marine-fixed nitrogen isotopic budget: Implications for Holocene nitrogen cycling. *Global Biogeochem. Cycles* **16**, 1120 (2002). doi:10.1029/2001GB001856

26. D. M. Sigman, P. J. DiFiore, M. P. Hain, C. Deutsch, Y. Wang, D. M. Karl, A. N. Knapp, M. F. Lehmann, S. Pantoja, The dual isotopes of deep nitrate as a constraint on the cycle and budget of oceanic fixed nitrogen. *Deep Sea Res. Part I* **56**, 1419–1439 (2009). doi:10.1016/j.dsr.2009.04.007

27. X. Zhou, E. Thomas, R. E. M. Rickaby, A. M. E. Winguth, Z. Lu, I/Ca evidence for upper ocean deoxygenation during the PETM. *Paleoceanography* **29**, 964–975 (2014). doi:10.1002/2014PA002702

28. M. Lyle, J. Barron, T. J. Bralower, M. Huber, A. Olivarez Lyle, A. C. Ravelo, D. K. Rea, P. A. Wilson, Pacific ocean and Cenozoic evolution of climate. *Rev. Geophys.* **46**, RG2002 (2008). doi:10.1029/2005RG000190

29. B. S. Cramer, J. R. Toggweiler, J. D. Wright, M. E. Katz, K. G. Miller, Ocean overturning since the late Cretaceous: Inferences from a new benthic foraminiferal isotope compilation. *Paleoceanography* **24**, PA4216 (2009). doi:10.1029/2008PA001683

30. W. Cao, S. Zahirovic, N. Flament, S. Williams, J. Golonka, R. D. Müller, Improving global paleogeography since the late Paleozoic using paleobiology. *Biogeosciences* **14**, 5425–5439 (2017). doi:10.5194/bg-14-5425-2017

31. X. Hu, E. Garzanti, J. Wang, W. Huang, W. An, A. Webb, The timing of India-Asia collision onset – Facts, theories, controversies. *Earth Sci. Rev.* **160**, 264–299 (2016). doi:10.1016/j.earscirev.2016.07.014

32. T. C. Chamberlin, On a possible reversal of deep-sea circulation and its influence on geologic climates. *J. Geol.* **14**, 363–373 (1906). doi:10.1086/621315

33. G. W. Brass, J. R. Southam, W. H. Peterson, Warm saline bottom water in the ancient ocean. *Nature* **296**, 620–623 (1982). doi:10.1038/296620a0

34. D. J. Thomas, R. L. Korty, M. Huber, J. A. Schubert, B. Haines, Nd isotopic structure of the Pacific Ocean 70–30 Ma and numerical evidence for vigorous ocean circulation and ocean heat transport in a greenhouse world. *Paleoceanography* **29**, 454–469 (2014). doi:10.1002/2013PA002535

35. T. D. Herbert, J. L. Sarmiento, Ocean nutrient distribution and oxygenation: Limits on the formation of warm saline bottom water over the past 91 m.y. *Geology* **19**, 702–705 (1991). doi:10.1130/0091-7613(1991)019<0702:ONDAOL>2.3.CO;2

36. K. L. Bice, E. J. Barron, W. H. Peterson, Continental runoff and early Cenozoic bottom-water sources. *Geology* **25**, 951–954 (1997). doi:10.1130/0091-7613(1997)025<0951:CRAECB>2.3.CO;2

37. A. Paytan, M. Kastner, D. Campbell, M. H. Thiemens, Sulfur isotopic composition of cenozoic seawater sulfate. *Science* **282**, 1459–1462 (1998). doi:10.1126/science.282.5393.1459 Medline

38. A. C. Kurtz, L. R. Kump, M. A. Arthur, J. C. Zachos, A. Paytan, Early Cenozoic decoupling of the global carbon and sulfur cycles. *Paleoceanography* **18**, 1090 (2003). doi:10.1029/2003PA000908

39. V. C. F. Rennie, G. Paris, A. L. Sessions, S. Abramovich, A. V. Turchyn, J. F. Adkins, Cenozoic record of $\delta^{34}S$ in foraminiferal calcite implies an early Eocene shift to deep-ocean sulfide burial. *Nat. Geosci.* **11**, 761–765 (2018). doi:10.1038/s41561-018-0200-y

40. S. Schouten, E. C. Hopmans, E. Schefuß, J. S. Sinninghe-Damsté, Distributional variations in marine crenarchaeotal membrane lipids: A new tool for reconstructing ancient sea water temperatures? *Earth Planet. Sci. Lett.* **204**, 265–274 (2002). doi:10.1016/S0012-821X(02)00979-2

41. A. Dutton, K. C. Lohmann, R. M. Leckie, Insights from the Paleogene tropical Pacific: Foraminiferal stable isotope and elemental results from Site 1209, Shatsky Rise. *Paleoceanography* **20**, PA3004 (2005). doi:10.1029/2004PA001098

42. A. J. P. Houben, C. A. van Mourik, A. Montanari, R. Coccioni, H. Brinkhuis, The Eocene-Oligocene transition: Changes in sea level, temperature or both? *Palaeogeogr. Palaeoecol.* **335–336**, 75–83 (2012). doi:10.1016/j.palaeo.2011.04.008

43. T. DeVries, C. Deutsch, P. A. Rafter, F. Primeau, Marine denitrification rates determined from a global 3-D inverse model. *Biogeosciences* **10**, 2481–2496 (2013). doi:10.5194/bg-10-2481-2013

44. P. B. Wignall, R. J. Twitchett, Oceanic anoxia and the end Permian mass extinction. *Science* **272**, 1155–1158 (1996). doi:10.1126/science.272.5265.1155 Medline

45. R. J. Matear, A. C. Hirst, Long-term changes in dissolved oxygen concentrations in the ocean caused by protracted global warming. *Global Biogeochem. Cycles* **17**, 1125 (2003). doi:10.1029/2002GB001997

46. M. Seton, R. D. Müller, S. Zahirovic, C. Gaina, T. Torsvik, G. Shephard, A. Talsma, M. Gurnis, M. Turner, S. Maus, M. Chandler, Global continental and ocean basin reconstructions since 200Ma. *Earth Sci. Rev.* **113**, 212–270 (2012). doi:10.1016/j.earscirev.2012.03.002

47. F. M. Gradstein, J. G. Ogg, M. Schmitz, G. Ogg, Eds., *The Geologic Time Scale 2012* (Elsevier, 2012).

48. J. E. Tierney, M. P. Tingley, A Bayesian, spatially-varying calibration model for the TEX_{86} proxy. *Geochim. Cosmochim. Acta* **127**, 83–106 (2014). doi:10.1016/j.gca.2013.11.026

49. J. Erez, B. Luz, Experimental paleotemperature equation for planktonic foraminifera. *Geochim. Cosmochim. Acta* **47**, 1025–1031 (1983). doi:10.1016/0016-7037(83)90232-6

50. M. R. Petrizzo, I. Premoli Silva, P. Ferrari, "Data report: Paleogene planktonic foraminifer biostratigraphy, ODP Leg 198 Holes 1209A, 1210A, and 1211A (Shatsky Rise, northwest Pacific Ocean)," *Proceedings of the Ocean Drilling Program, Scientific Results*, vol. 198 (2005).

51. T. J. Bralower, "Data report: Paleocene–early Oligocene calcareous nannofossil biostratigraphy, ODP Leg 198 Sites 1209, 1210, and 1211 (Shatsky Rise, Pacific Ocean)," *Proceedings of the Ocean Drilling Program, Scientific Results*, vol. 198 (2005).

52. J. Bowles, "Data report: Revised magnetostratigraphy and magnetic mineralogy of sediments from Walvis Ridge, Leg 208," *Proceedings of the Ocean Drilling Program, Scientific Results*, vol. 208 (2006).

53. K. L. Casciotti, T. W. Trull, D. M. Glover, D. Davies, Constraints on nitrogen cycling at the subtropical North Pacific Station ALOHA from isotopic measurements of nitrate and particulate nitrogen. *Deep Sea Res. Part II* **55**, 1661–1672 (2008). doi:10.1016/j.dsr2.2008.04.017

54. H. Ren, D. M. Sigman, A. Martínez-García, R. F. Anderson, M. T. Chen, A. C. Ravelo, M. Straub, G. T. F. Wong, G. H. Haug, Impact of glacial/interglacial sea level change on the ocean nitrogen cycle. *Proc. Natl. Acad. Sci. U.S.A.* **114**, E6759–E6766 (2017). doi:10.1073/pnas.1701315114 Medline

55. K. M. Costa, J. F. McManus, R. F. Anderson, H. Ren, D. M. Sigman, G. Winckler, M. Q. Fleisher, F. Marcantonio, A. C. Ravelo, No iron fertilization in the equatorial Pacific Ocean during the last ice age. *Nature* **529**, 519–522 (2016). doi:10.1038/nature16453 Medline

56. O. P. Mehra, M. L. Jackson, Iron oxide removal from soils and clays by a dithionite citrate system buffered with sodium bicarbonate. *Clays Clay Miner.* **7**, 317–327 (1958). doi:10.1346/CCMN.1958.0070122

57. X. T. Wang, D. M. Sigman, A. L. Cohen, D. J. Sinclair, R. M. Sherrell, M. A. Weigand, D. V. Erler, H. Ren, Isotopic composition of skeleton-bound organic nitrogen in reef-building symbiotic corals: A new method and proxy evaluation at Bermuda. *Geochim. Cosmochim. Acta* **148**, 179–190 (2015). doi:10.1016/j.gca.2014.09.017

58. D. M. Sigman, K. L. Casciotti, M. Andreani, C. Barford, M. Galanter, J. K. Böhlke, A bacterial method for the nitrogen isotopic analysis of nitrate in seawater and freshwater. *Anal. Chem.* **73**, 4145–4153 (2001). doi:10.1021/ac010088e Medline

59. M. A. Weigand, J. Foriel, B. Barnett, S. Oleynik, D. M. Sigman, Updates to instrumentation and protocols for isotopic analysis of nitrate by the denitrifier method. *Rapid Commun. Mass Spectrom.* **30**, 1365–1383 (2016). doi:10.1002/rcm.7570 Medline

60. F. Nydahl, On the peroxodisulphate oxidation of total nitrogen in waters to nitrate. *Water Res.* **12**, 1123–1130 (1978). doi:10.1016/0043-1354(78)90060-X

61. H. Qi, T. B. Coplen, H. Geilmann, W. A. Brand, J. K. Böhlke, Two new organic reference materials for $\delta^{13}C$ and $\delta^{15}N$ measurements and a new value for the $\delta^{13}C$ of NBS 22 oil. *Rapid Commun. Mass Spectrom.* **17**, 2483–2487 (2003). doi:10.1002/rcm.1219 Medline

62. A. Schimmelmann, H. Qi, T. B. Coplen, W. A. Brand, J. Fong, W. Meier-Augenstein, H. F. Kemp, B. Toman, A. Ackermann, S. Assonov, A. T. Aerts-Bijma, R. Brejcha, Y. Chikaraishi, T. Darwish, M. Elsner, M. Gehre, H. Geilmann, M. Gröning, J. F. Hélie, S. Herrero-Martín, H. A. Meijer, P. E. Sauer, A. L. Sessions, R. A. Werner, Organic reference materials for hydrogen, carbon, and nitrogen stable isotope-ratio measurements: Caffeines, n-alkanes, fatty acid methyl esters, glycines, L-valines, polyethylenes, and oils. *Anal. Chem.* **88**, 4294–4302 (2016). doi:10.1021/acs.analchem.5b04392 Medline

63. R. S. Braman, S. A. Hendrix, Nanogram nitrite and nitrate determination in environmental and biological materials by vanadium (III) reduction with chemiluminescence detection. *Anal. Chem.* **61**, 2715–2718 (1989). doi:10.1021/ac00199a007 Medline

64. J. K. Böhlke, T. B. Coplen, “Interlaboratory comparison of reference materials for nitrogen-isotope-ratio measurements” in *Reference and Intercomparison Materials for Stable Isotopes of Light Elements* (International Atomic Energy Agency, 1995), pp. 51–66.

65. A. P. Patwardhan, D. H. Thompson, Efficient synthesis of 40- and 48-membered tetraether macrocyclic bisphosphocholines. *Org. Lett.* **1**, 241–244 (1999). doi:10.1021/ol990567o Medline

66. C. Huguet, E. C. Hopmans, W. Febo-Ayala, D. H. Thompson, J. S. Sinninghe Damsté, S. Schouten, An improved method to determine the absolute abundance of glycerol dibiphytanyl glycerol tetraether lipids. *Org. Geochem.* **37**, 1036–1041 (2006). doi:10.1016/j.orggeochem.2006.05.008

67. E. C. Hopmans, S. Schouten, J. S. Sinninghe Damsté, The effect of improved chromatography on GDGT-based palaeoproxies. *Org. Geochem.* **93**, 1–6 (2016). doi:10.1016/j.orggeochem.2015.12.006

68. J. Kim, J. van der Meer, S. Schouten, P. Helmke, V. Willmott, F. Sangiorgi, N. Koç, E. C. Hopmans, J. S. S. Damsté, New indices and calibrations derived from the distribution of crenarchaeal isoprenoid tetraether lipids: Implications for past sea surface temperature reconstructions. *Geochim. Cosmochim. Acta* **74**, 4639–4654 (2010). doi:10.1016/j.gca.2010.05.027

69. E. C. Hopmans, J. W. H. Weijers, E. Schefuß, L. Herfort, J. S. Sinninghe Damsté, S. Schouten, A novel proxy for terrestrial organic matter in sediments based on branched and isoprenoid tetraether lipids. *Earth Planet. Sci. Lett.* **224**, 107–116 (2004). doi:10.1016/j.epsl.2004.05.012

70. J. W. H. Weijers, S. Schouten, O. C. Spaargaren, J. S. Sinninghe Damsté, Occurrence and distribution of tetraether membrane lipids in soils: Implications for the use of the TEX_{86} proxy and the BIT index. *Org. Geochem.* **37**, 1680–1693 (2006). doi:10.1016/j.orggeochem.2006.07.018

71. Y. Koga, M. Akagawa-Matsushita, M. Ohga, M. Nishihara, Taxonomic significance of the distribution of component parts of polar ether lipids in methanogens. *Syst. Appl. Microbiol.* **16**, 342–351 (1993). doi:10.1016/S0723-2020(11)80264-X

72. C. I. Blaga, G. Reichart, O. Heiri, J. S. Sinninghe Damsté, Tetraether membrane lipid distributions in water-column particulate matter and sediments: A study of 47 European lakes along a north–south transect. *J. Paleolimnol.* **41**, 523–540 (2009). doi:10.1007/s10933-008-9242-2

73. R. D. Pancost, E. C. Hopmans, J. S. Sinninghe Damsté, Archaeal lipids in Mediterranean cold seeps: Molecular proxies for anaerobic methane oxidation. *Geochim. Cosmochim. Acta* **65**, 1611–1627 (2001). doi:10.1016/S0016-7037(00)00562-7

74. Y. G. Zhang, C. L. Zhang, X.-L. Liu, L. Li, K.-U. Hinrichs, J. E. Noakes, Methane Index: A tetraether archaeal lipid biomarker indicator for detecting the instability of marine gas hydrates. *Earth Planet. Sci. Lett.* **307**, 525–534 (2011). doi:10.1016/j.epsl.2011.05.031

75. Y. G. Zhang, M. Pagani, Z. Wang, Ring Index: A new strategy to evaluate the integrity of TEX_{86} paleothermometry. *Paleoceanography* **31**, 220–232 (2016). doi:10.1002/2015PA002848

76. K. Kritee, D. M. Sigman, J. Granger, B. B. Ward, A. Jayakumar, C. Deutsch, Reduced isotope fractionation by denitrification under conditions relevant to the ocean. *Geochim. Cosmochim. Acta* **92**, 243–259 (2012). doi:10.1016/j.gca.2012.05.020

77. D. Marconi, S. Kopf, P. A. Rafter, D. M. Sigman, Aerobic respiration along isopycnals leads to overestimation of the isotope effect of denitrification in the ocean water column. *Geochim. Cosmochim. Acta* **197**, 417–432 (2017). doi:10.1016/j.gca.2016.10.012

78. A. Bourbonnais, M. A. Altabet, C. N. Charoenpong, J. Larkum, H. Hu, H. W. Bange, L. Stramma, N-loss isotope effects in the Peru oxygen minimum zone studied using a mesoscale eddy as a natural tracer experiment. *Global Biogeochem. Cycles* **29**, 793–811 (2015). doi:10.1002/2014GB005001

79. P. N. Pearson, B. E. van Dongen, C. J. Nicholas, R. D. Pancost, S. Schouten, J. M. Singano, B. S. Wade, Stable warm tropical climate through the Eocene Epoch. *Geology* **35**, 211–214 (2007). doi:10.1130/G23175A.1

80. D. P. Schrag, D. J. DePaolo, F. M. Richter, Reconstructing past sea surface temperatures: Correcting for diagenesis of bulk marine carbonate. *Geochim. Cosmochim. Acta* **59**, 2265–2278 (1995). doi:10.1016/0016-7037(95)00105-9

81. P. N. Pearson, P. W. Ditchfield, J. Singano, K. G. Harcourt-Brown, C. J. Nicholas, R. K. Olsson, N. J. Shackleton, M. A. Hall, Warm tropical sea surface temperatures in the Late Cretaceous and Eocene epochs. *Nature* **413**, 481–487 (2001). doi:10.1038/35097000 Medline

82. J. I. Hedges, R. G. Keil, Sedimentary organic matter preservation: An assessment and speculative synthesis. *Mar. Chem.* **49**, 81–115 (1995). doi:10.1016/0304-4203(95)00008-F

83. H. E. Hartnett, R. G. Keil, J. I. Hedges, A. H. Devol, Influence of oxygen exposure time on organic carbon preservation in continental margin sediments. *Nature* **391**, 572–575 (1998). doi:10.1038/35351

84. D. J. J. van Hinsbergen, L. V. de Groot, S. J. van Schaik, W. Spakman, P. K. Bijl, A. Sluijs, C. G. Langereis, H. Brinkhuis, A Paleolatitude Calculator for Paleoclimate Studies. *PLOS ONE* **10**, e0126946 (2015). doi:10.1371/journal.pone.0126946 Medline

85. J. S. Sinninghe Damsté, J. Ossebaar, S. Schouten, D. Verschuren, Distribution of tetraether lipids in the 25-ka sedimentary record of Lake Challa: Extracting reliable TEX_{86} and MBT/CBT palaeotemperatures from an equatorial African lake. *Quat. Sci. Rev.* **50**, 43–54 (2012). doi:10.1016/j.quascirev.2012.07.001